Electronic Supplementary Information (ESI)

Regioselective synthesis, isomerisation, *in vitro* oestrogen activity, and copolymerisation of bisguaicol F (BGF) isomers

S.-F Koelewijn,*[a] D. Ruijten,[a] L. Trullemans,[a] Tom Renders,[a] P. Van Puyvelde,[b] H. Witters,[c] and B. F. Sels*[a]

[a] Dept. of Microbial and Molecular Systems (M^2S), Center for Sustainable Catalysis and Engineering (CSCE), KU Leuven, Celestijnenlaan 200F, 3001 Leuven, Belgium
[b] Dept. of Chemical Engineering, Soft Matter, Rheology and Technology (SMaRT), KU Leuven, Celestijnenlaan 200F, 3001 Leuven, Belgium
[c] Dept. of Health, Applied Bio & molecular Systems (ABS), Flemish Institute for Technological Research (VITO), Boeretang 200, 2400 Mol, Belgium

*Corresponding authors. E-mail: stef.koelewijn@kuleuven.be; bert.sels@kuleuven.be

I. Materials and methods

Chemicals and materials

All commercial chemicals were analytical reagents and were used without further purification. Amberlyst®-15 dry (4.7 mmol H^+/g, moisture ≤ 1.5%, <300 µm), silica gel (pore size 60 Å, 70-230 mesh, 63-200 µm), potassium bromide (KBr, ≥99.0%), phenol (≥99%), guaiacol (99+%), vanillyl alcohol (≥98%), isovanillyl alcohol (98%), creosol (2-methoxy-4-methylphenol, ≥98%), *N*-methyl-*N*-(trimethylsilyl) trifluoroacetamide (MSTFA, ≥98.5%), anhydrous pyridine (99.8%), dichloromethane (DCM, >99%), tetrahydrofuran (THF, >99%), trifluoroacetic acid-*d* (TFA-*d*, 99.5 atom % D), chloroform-*d* ($CDCl_3$, 99.8 atom % D, contains 0.03 vol.% TMS), triethylamine (≥99%), 17β-oestradiol (17β-E2, >98%), tetrabutylammonium chloride (≥97%), *para*-toluenesulfonic acid monohydrate (*p*-TSA, 98.5%), and crystalline triphosgene [bis(trichloromethyl)carbonate, BTC, 98%] were purchased from **Sigma-Aldrich**. Concentrated hydrochloric acid (HCl, 37 wt.%), sodium hydroxide (NaOH, 99.4%), anhydrous magnesium sulphate ($MgSO_4$, >99%) and anhydrous acetone (≥99.5%) were purchased from **Fisher Scientific**. Bisphenol A [BPA, 2,2'-bis(4-hydroxyphenyl)propane, >99.0%], bisphenol F [BPF, 1,1'-bis(4-hydroxyphenol)methane, >99%] and *ortho*-vanillylalcohol (>98%) were purchased from **TCI Europe**. Acetonitrile (ACN, 99.9+%) and *n*-heptane (99+%) were purchased from **Acros Organics**. Oestrogen-free dimethyl sulfoxide (DMSO, 99.5%) was purchased from **Labscan**. Water was purified using a Millipore Milli-Q Advantage A10 water purification system to a resistivity higher than 18 MΩ·cm at 25 °C.

Methods and procedures

In vitro oestrogenic potency screening

The experiments were done as formerly reported by Witters *et al.* (2010) with some alterations.[1]

» MELN cells

MELN cells (provided by INSERM, Montpellier, FR; Balaguer *et al.* (1999)) are oestrogen-sensitive human breast cancer cells (MCF-7) stably transfected with the oestrogen-responsive gene (ERE-βGlo-Luc-SVNeo) carried by integrated plasmids.[2] In addition to the antibiotic resistance selection gene (SVNeo), these plasmids also contain oestrogen-responsive elements to which the oestrogen receptor (hERα)-ligand complex can bind, hence inducing the transcription of the luciferase reporter gene. MELN cells were cultured in DMEM:F12 medium with GlutaMax™ I supplemented with 1% penicillin/streptomycin (all Gibco, ThermoFisher, Ghent, BE), 1 mg.mL^{-1} G418 sulphate (Invivogen, Toulouse, FR) and 7.5% fetal bovine serum superior (Biochrome, Gentaur, Kampenhout, BE). The cell line was maintained in an incubator at 37 °C, a relative humidity of 95% and a CO_2 concentration of 5%.

» Exposure of cells

A standard set-up has been developed to expose MELN cells and measure ER-transactivation for xeno-oestrogenic compounds. In order to decrease the background signal, cells were adapted to charcoal/dextran treated fetal calf serum (Gibco, ThermoFisher, Ghent, BE). Cells were seeded at a density of $8 \cdot 10^5$ cells per well, in oestrogen-free black 96-well plates with transparent bottoms (Costar). Cells were maintained in 100 µL test medium for 24 h. Serial dilutions of the test compounds were made in oestrogen-free DMSO. Dilutions of the test compound were added to the test medium and 100 µL of each concentration was added to three replica wells. The final solvent concentration was always 0.1 vol.%. Cells were treated with the test compounds for 19-20 h. Each bisphenol/bisguaicol compound was studied in a range finding experiment ($1.00 \cdot 10^{-10}$–$1.00.10^{-3}$ M; see Table S1), and subsequent repeat experiments in an appropriate working range to determine EC_{50} (see *Data Analyses*). In each experiment, for each concentration three replica wells were tested. Test compounds were assessed in comparison to a positive assay control (17β-E2), and the known positive industrial compounds BPA and BPF.

» Luciferase assay

At the end of the incubation period, the remaining medium is removed for analysis of cell damage using the CytoTox-ONE™ Homogenous Membrane Integrity Assay (Promega) as previously described by Berckmans *et al.* (2007).[3] Next, cells were lysed by

adding 30 µL reporter lysis buffer (Promega, Leiden, NL) in each well. After shaking plates for 25 min, plates were frozen (-80 °C) for minimum 1 h and maximum 1 week. After thawing the plates, luminescence was measured using a luminometer (Luminoskan) after injection of 50 µL luciferase reagent (Promega, Leiden, NL) in each well. Results are expressed as relative light units (RLU).

» Data analysis

Results are presented as induction of hERα activation expressed as percentage of luciferase induction by the vehicle control (set at 100%). Results from three replicates were input to Graphpad Prism software (v7.03, 2017), and graphs were fitted based on mean values ± SD, while EC_{50} values were determined by fitting a four-parameter sigmoidal dose-response curve (*cf*. Hill equation). To obtain EC_{50} values for partial dose-response curves, the fit was constrained at the top value. Few compounds exhibited cytotoxicity at the highest concentrations (10^{-3} M; see Table S1); if present, these results were excluded in the fit. The EC_{50} values allow to rank the compounds for their potency (*i.e.* higher EC_{50}, less potent). To calculate the relative oestrogenic potency (REP), the EC_{50} for reference 17β-E2 was divided by the EC_{50} for each bisphenol/bisguaiacol, and expressed as percentage. To calculate REE, the E_{max} for each bisphenol/bisguaiacol was divided by the E_{max} for reference 17β-E2, and expressed as percentage. While EC_{50} and E_{max} values only allow intra-experimental comparison of potency and efficacy, REP and REE values allow both intra- and inter-experimental comparison. Notice that data of BPA were derived from a previous experiment with 17β-E2 values (EC_{50} = $4.3 \cdot 10^{-11}$ M; E_{max} = 456%) in a similar range.[4]

Statistics on observed ^{13}C carbonyl resonances distribution

Instead of one distinct ^{13}C carbonyl resonance as seen for the *p,p'*-BGF-PC homopolymer, the ^{13}C NMR spectra of the *m,p'*-BGF-PC homopolymer and the BGF-*co*-PC copolymer display three neighboring resonances (within ±0.4 ppm). Namely, while homopolymers of *p,p'*-BGF can afford only one type of carbonate linkages (*i.e.* p – p), copolymers of *p,p'*- and *m,p'*-BGF can yield three types of carbonate linkages (*i.e.* p – p, p – m and m – m). To corroborate that these differences in linkages are indeed the reason for the distinct resonance splitting, the linkage distribution was approximated by statistical analysis for a 'polymer' with a degree of polymerisation of 2 (*i.e.* dimer formation).

fraction of p – p = [(probability for p – p from *p,p*' + *p,p*') * (probability for *p,p*' * probability for *p,p*')] +
[(probability for p – p from *p,p*' + *m,p*') * 2*(probability for *p,p*' * probability for *m,p*')] +
[(probability for p – p from *m,p*' + *m,p*') * (probability for *m,p*' * probability for *m,p*')]

fraction of m – p = [(probability for m – p from *p,p*' + *m,p*') * 2*(probability for *p,p*' * probability for *m,p*')] +
[(probability for m – p from *m,p*' + *m,p*') * (probability for *m,p*' * probability for *m,p*')]

fraction of m – m = [(probability for m – m from *m,p*' + *m,p*') * (probability for *m,p*' * probability for *m,p*')]

Type of (co)polymer	Type(s) of possible carbonate linkages	Estimated statistical distribution of carbonate linkages
p,p'-BGF-PC	only p – p	100% p – p
BGF-*co*-PC (25% *m,p*')	p – p, p – m and m – m	77% p – p, 22% p – m, 1% m – m
BGF-*co*-PC (50% *m,p*')	p – p, p – m and m – m	56% p – p, 38% p – m, 6% m – m
BGF-*co*-PC (75% *m,p*')	p – p, p – m and m – m	39% p – p, 47% p – m, 14% m – m
m,p'-BGF-PC	p – p, p – m and m – m	25% p – p, 50% p – m, 25% m – m

II. Figures

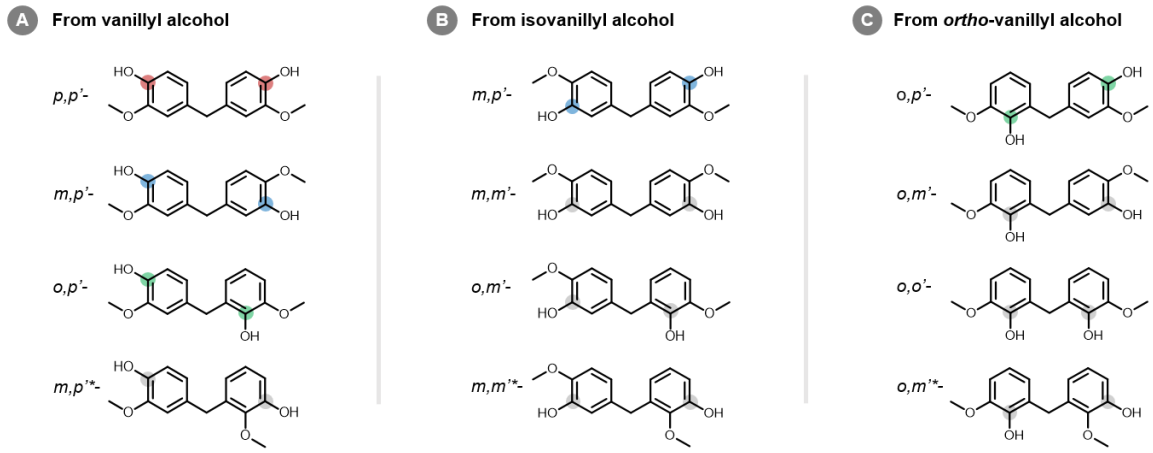

Fig. S1 | Overview of all theoretically possible BGF isomers formed from (**A**) *p*-VA, (**B**) *m*-VA, and (**C**) *o*-VA, as shown in expected order of abundance (top = high, bottom = low). Linkage nomenclature is based on the position of aryl hydroxyl to the methylene bridge, and indicated by dots for clarity. Coloured dots are used for *p,p'*- (**red**), *m,p'*- (**blue**) and *o,p'*-BGF (**green**). * Less-abundant isomers with identical linkage but different chemical structure.

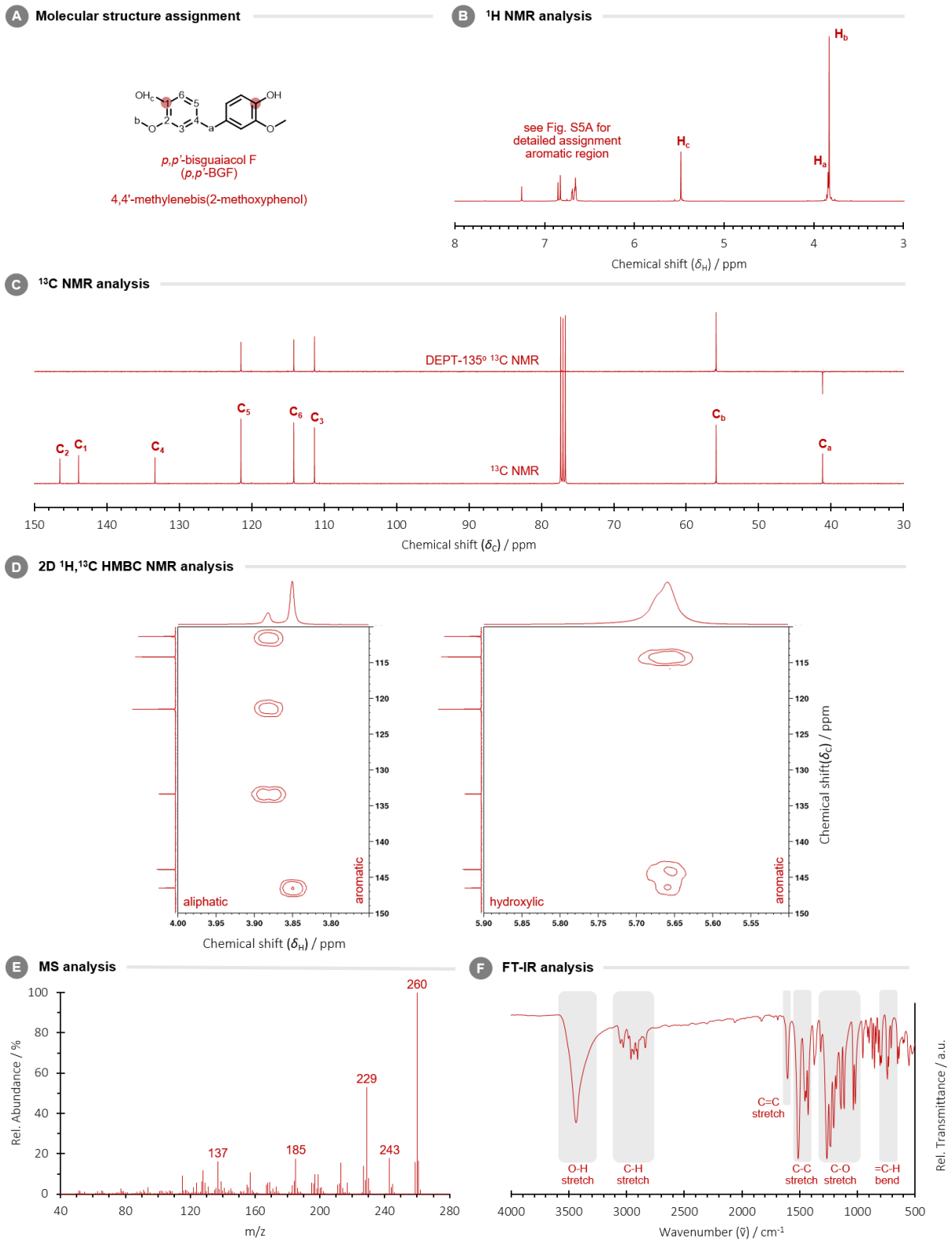

Figure S2 | Assignment of the molecular structure of *p,p'*-BGF (**A**) as corroborated by ^{1}H-NMR in $CDCl_3$ at 300 MHz (**B**), ^{13}C-NMR in $CDCl_3$ at 400 MHz (**C**), 2D ^{1}H,^{13}C HMBC NMR in $CDCl_3$ at 400 MHz (**D**), (GC-)MS with electron ionisation (**E**) and FT-IR spectroscopy *via* the KBr pellet method (**F**). Notice the structural symmetry of *p,p'*-BGF as observed by NMR resulting in only six ^{1}H resonances and eight ^{13}C resonances.

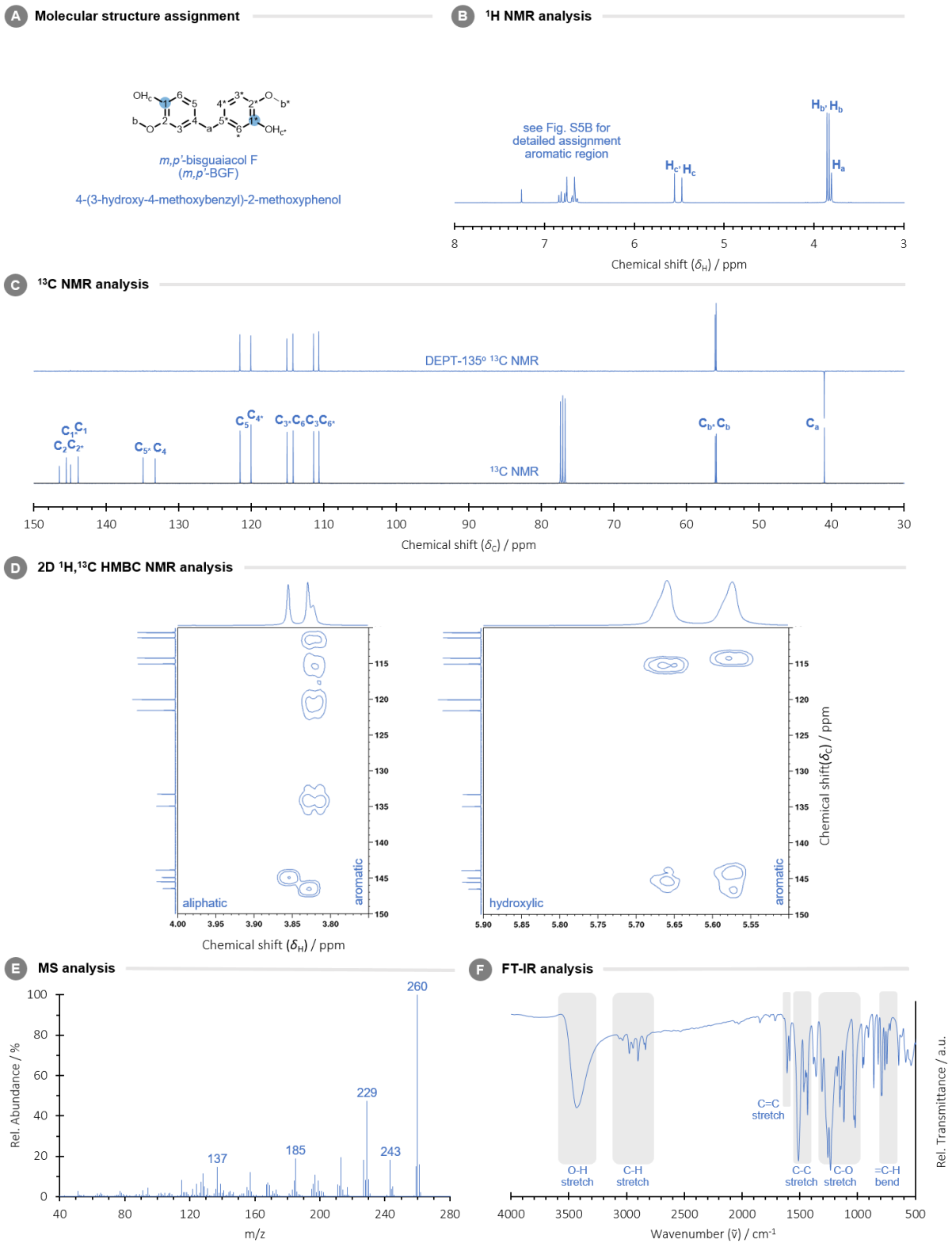

Figure S3 | Assignment of the molecular structure of *m,p'*-BGF (**A**) as corroborated by ^{1}H-NMR in $CDCl_3$ at 300 MHz (**B**), ^{13}C-NMR in $CDCl_3$ at 400 MHz (**C**), 2D ^{1}H,^{13}C HMBC NMR in $CDCl_3$ at 400 MHz (**D**), (GC-)MS with electron ionisation (**E**) and FT-IR spectroscopy *via* the KBr pellet method (**F**). Notice the structural asymmetry of *m,p'*-BGF as observed by NMR resulting in 11 ^{1}H resonances and 15 ^{13}C resonances.

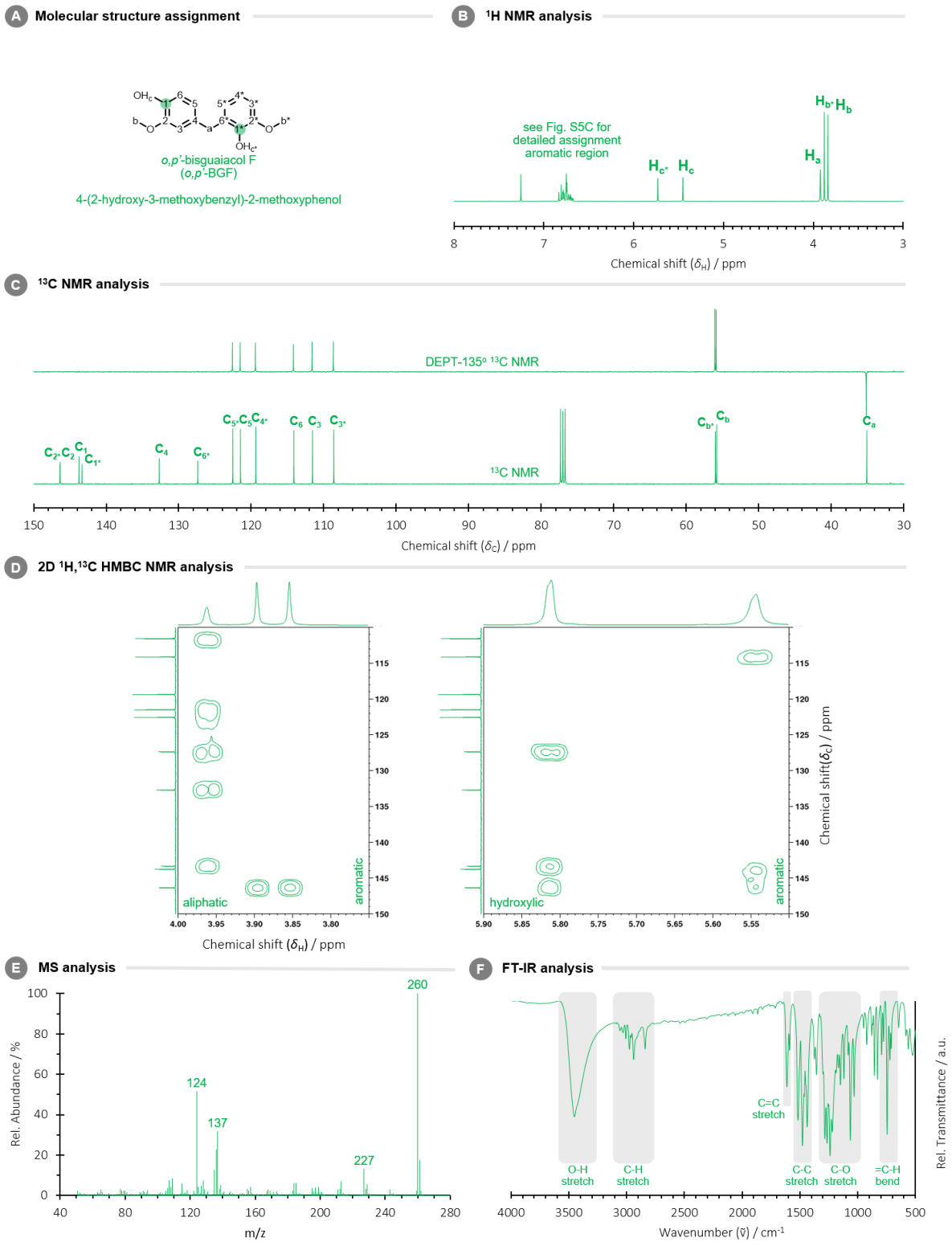

Figure S4 | Assignment of the molecular structure of *o,p'*-BGF (**A**) as corroborated by ^{1}H-NMR in $CDCl_3$ at 300 MHz (**B**), ^{13}C-NMR in $CDCl_3$ at 400 MHz (**C**), 2D ^{1}H,^{13}C HMBC NMR in $CDCl_3$ at 400 MHz (**D**), (GC-)MS with electron ionisation (**E**) and FT-IR spectroscopy *via* the KBr pellet method (**F**). Notice the structural asymmetry of *o,p'*-BGF as observed by NMR resulting in 11 ^{1}H resonances and 15 ^{13}C resonances.

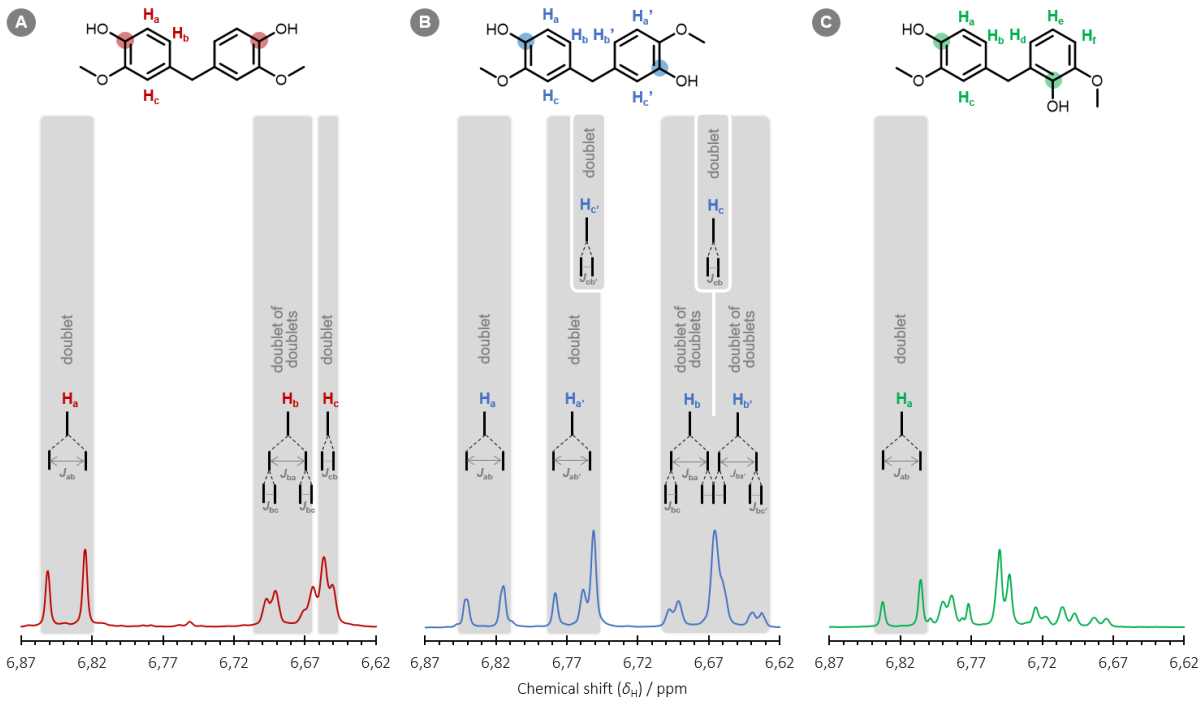

Figure S5 | Assignment of the aromatic ring protons by ^{1}H-NMR coupling pattern analysis of (**A**) *p,p'*- (red), (**B**) *m,p'* (blue), and (**C**) *o,p'*-BGF (green) as measured in $CDCl_3$ at 300 MHz. The structural symmetry of *p,p'*-BGF results in only three ^{1}H resonances instead of six resonances for asymmetric *m,p'*- and *o,p'*-BGF. For the multiplet of *o,p'*-BGF – comprising four doublets of doublets – only partial assignment was done.

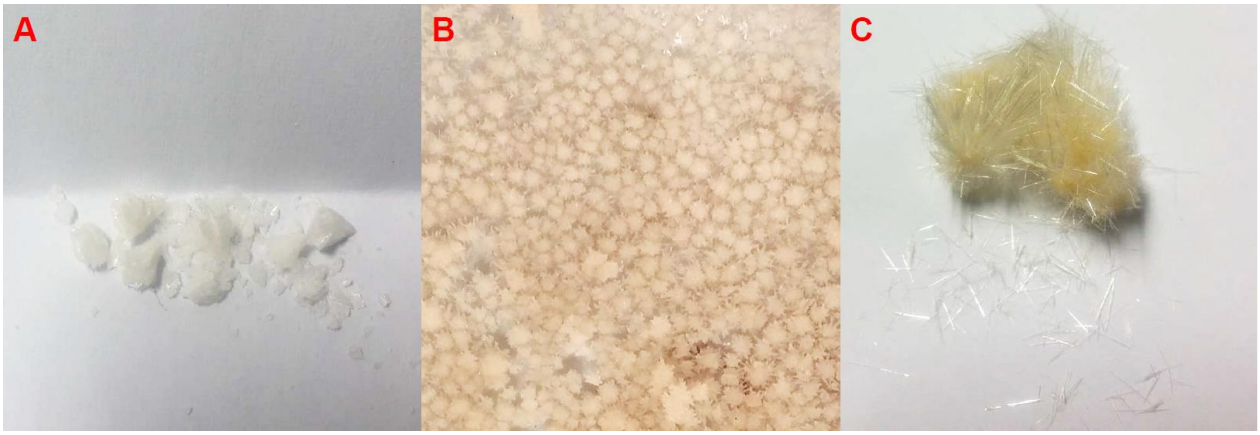

Figure S6 | Physical appearance of pure crystals (>99.5 %) of (**A**) *o,p'*-, (**B**) *m,p'*- and (**C**) *p,p'*-BGF regioisomers.

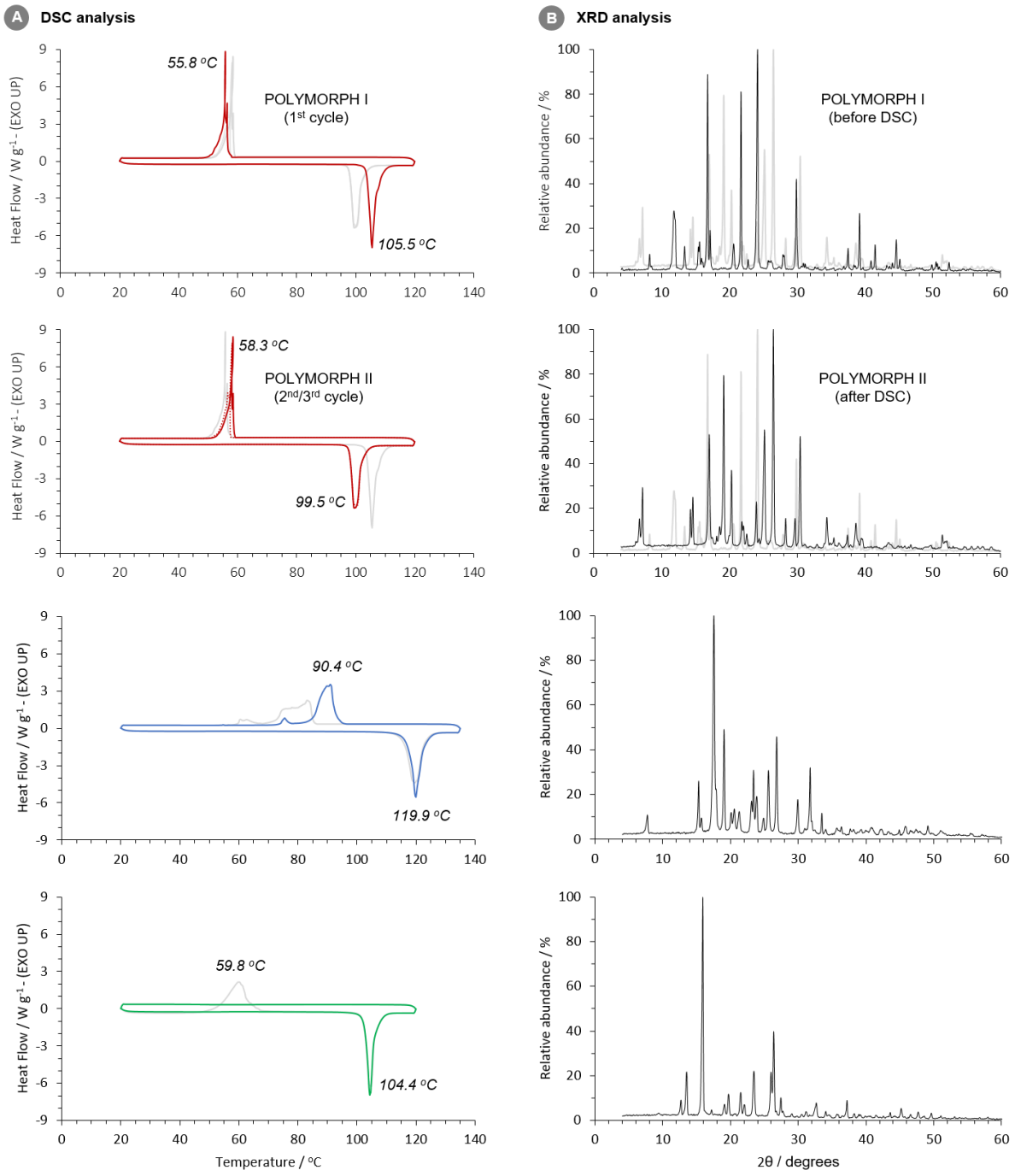

Figure S7 | Evidence for crystallinity in purified *p,p'*-BGF (red), *m,p'*-BGF (blue) and *o,p'*-BGF (green) regioisomers as observed by (**A**) DSC and confirmed by (**B**) XRD. Two polymorphs were observed for *p,p'*-BGF, which explains the existing melting point discrepancy in literature.[5,6] Unless denoted otherwise, the 1st and 2nd heating/cooling cycles are displayed in grey and colour, respectively. For *p,p'*-BGF, grey is used to indicate/compare morphologies (and not necessarily to indicate the 1st cycle).

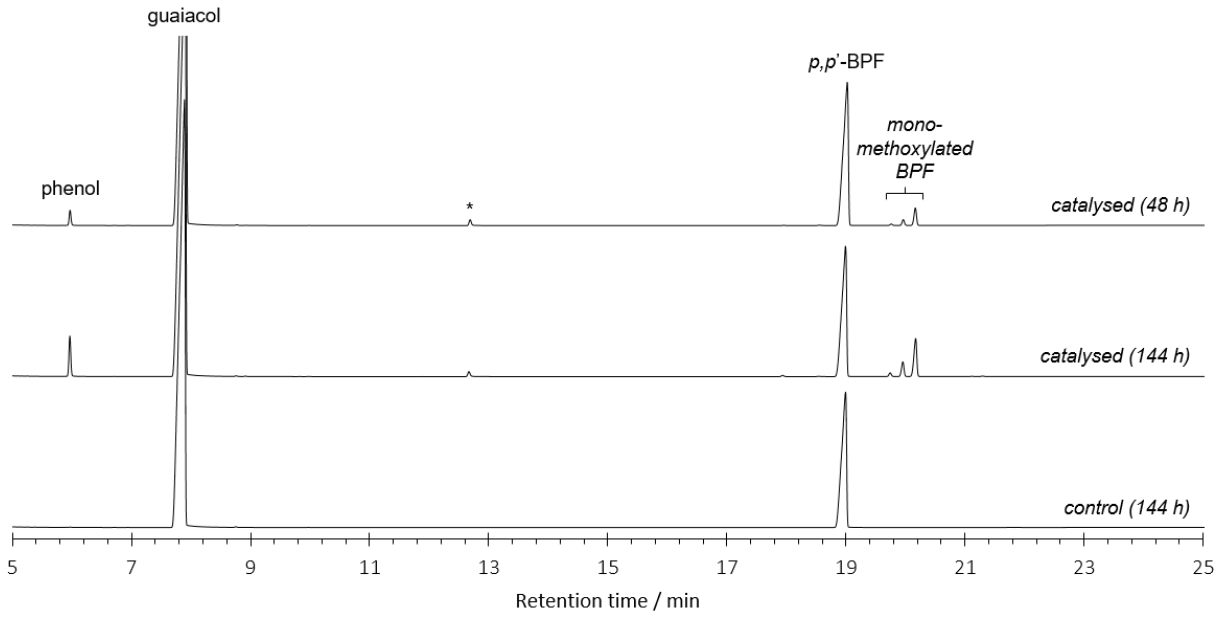

Figure S8 | GC-FID chromatograms after reacting isomerically pure *p,p'*-BPF with guaiacol in the presence or absence (*i.e.* control) of a homogeneous sulfonic acid (*i.e. p*-TSA) after 48 h and 144 h. Reaction conditions: 14 mmol guaiacol, 2 mmol *p,p'*-BPF, 0.12 mmol H^+, 80 °C. * Undetectable during GC-MS analysis, but likely a monoaromatic carbocation intermediate.

Figure S9 | Physical appearance of dried, precipitated polycarbonates. From **left to right**: BPA-PC ($\bar{M}_w$ = 16 kDa), BPA-PC ($\bar{M}_w$ = 126 kDa), *p,p'*-BGF-PC, BGF-*co*-PC (25% *m,p'*), BGF-*co*-PC (50% *m,p'*), BGF-*co*-PC (75% *m,p'*), *m,p'*-BGF-PC and BPF-PC.

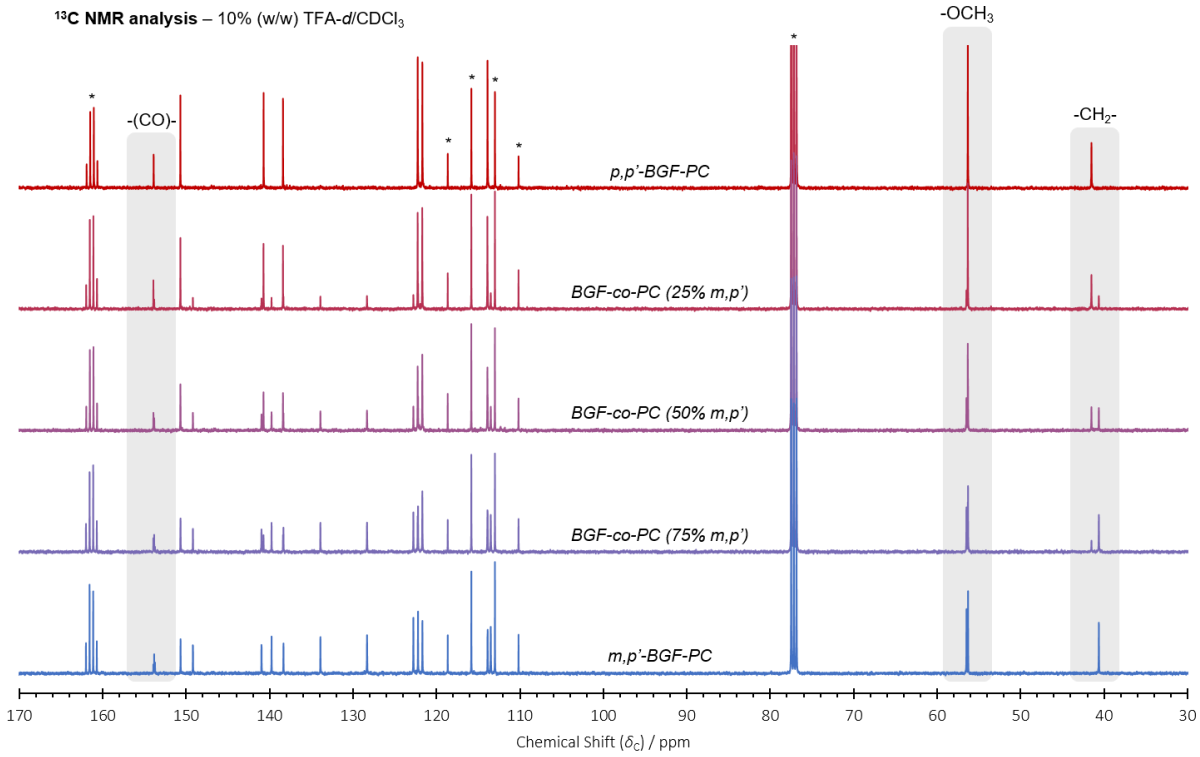

Figure S10 | ^{13}C NMR spectra of BGF-(*co*-)PCs in 10% (w/w) TFA-*d*/$CDCl_3$ at 400 MHz. Enlargements of carbonate (155–153 ppm), methoxyl (57–55 ppm) and methylene (42–40 ppm) carbon regions are provided in Fig. 6A-C, and the generalised molecular structure is proposed in Fig. 6D. * Residual solvent resonances at 164.2 (q) and 116.6 (q) for TFA and at 77.2 (t) ppm for $CHCl_3$.

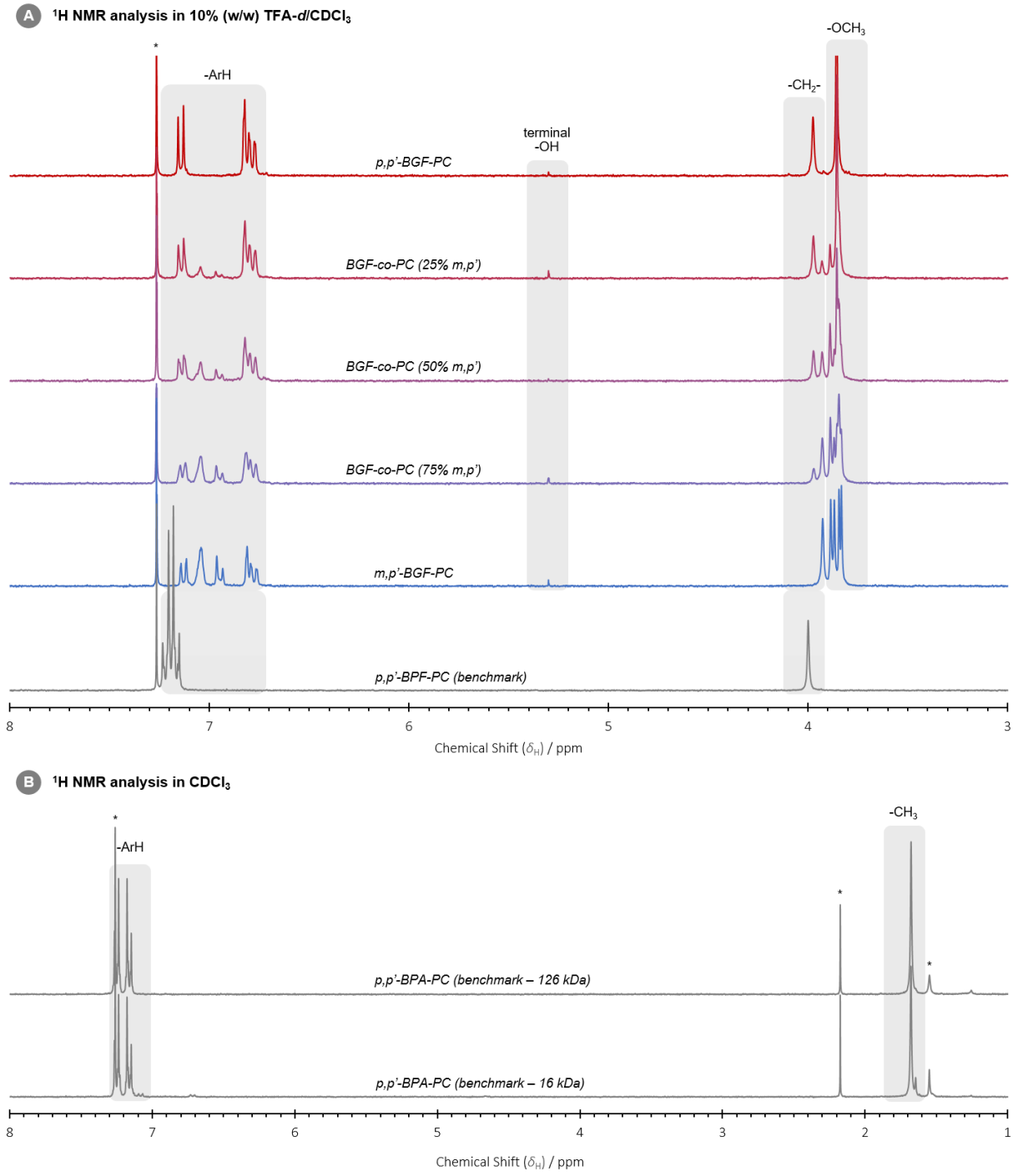

Figure S11 | ^{1}H NMR spectra at 300 MHz of (**A**) BGF-(*co*-)PC and BPF-PC polymers in 10% (w/w) TFA-*d*/$CDCl_3$, and (**B**) BPA-PC polymers in $CDCl_3$ with assignment of functional groups. Notice that the distribution of methylene (-CH_2-) resonances in BGF-*co*-PCs perfectly matches the initial monomer composition. The presence of –OH resonances for BGF-PCs is attributed to residual monomer species and not to terminal OH species as these –OH resonances were absent for low M_w BPA-PC. * Residual solvent resonances at 11.38 (s; not shown) for TFA, at 7.26 (s) for $CHCl_3$, at 2.17 (s) for acetone, and at 1.55 (s) ppm for water. For corresponding molecular structures see Fig. 6 and Fig. S12.

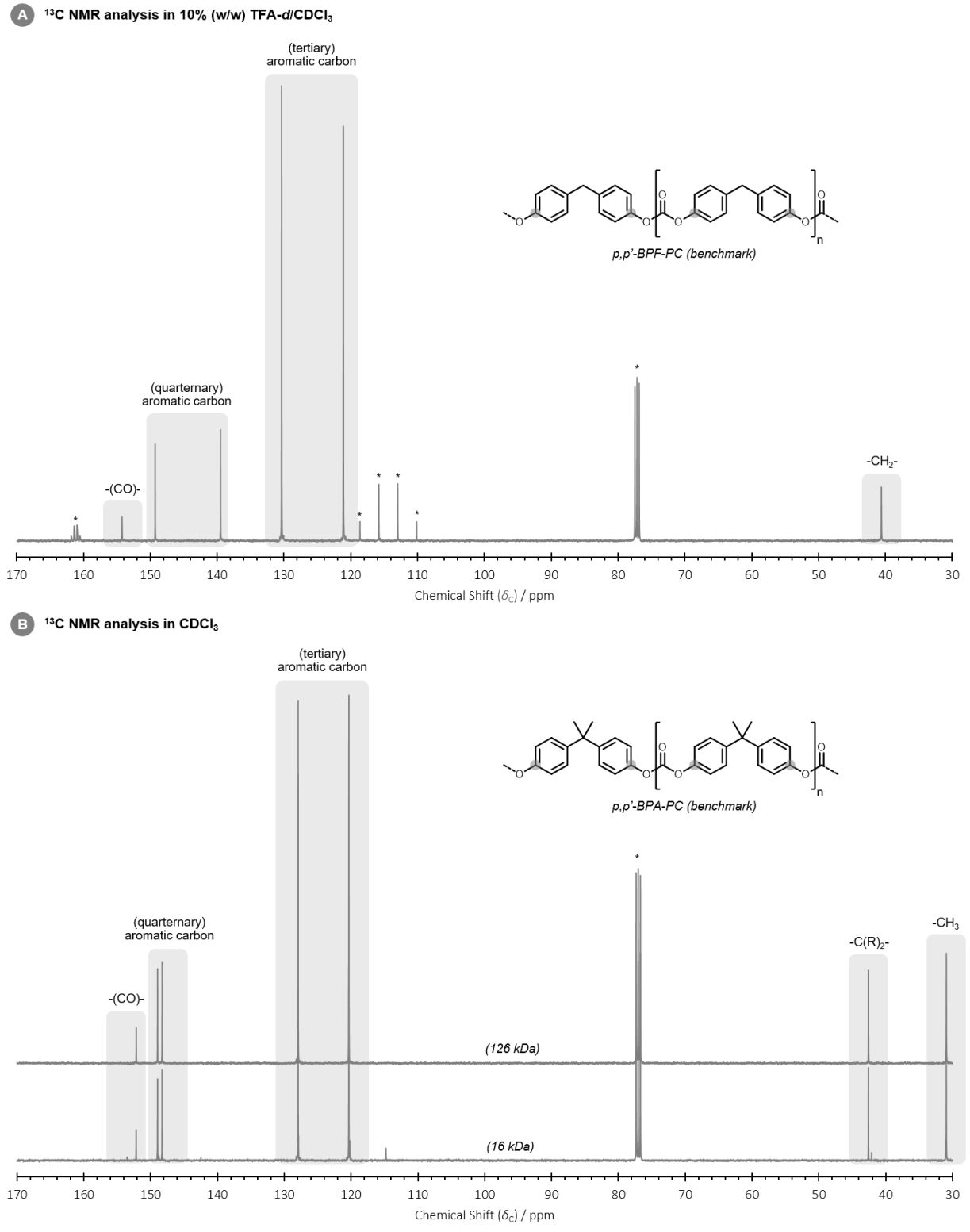

Figure S12 | ^{13}C NMR spectra of (**A**) (benchmark) BPF-PC in 10% (w/w) TFA-*d*/$CDCl_3$ at 400 MHz, and (**B**) (benchmark) BPA-PC polymers in $CDCl_3$ at 400 MHz with assignment of functional groups. * Residual solvent resonances at 164.2 (q) and 116.6 (q) for TFA and at 77.2 (t) ppm for $CHCl_3$.

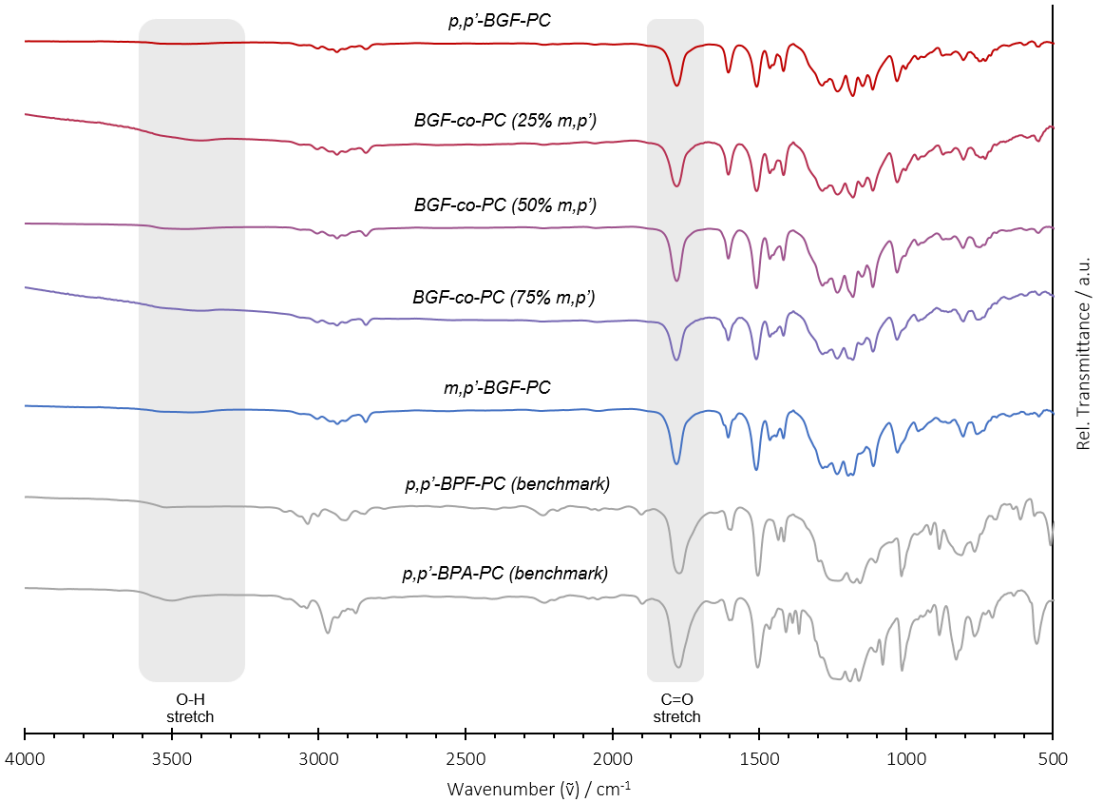

Fig. S13 | FT-IR spectra of BGF-(*co*-)PC benchmarked against BPF-PC and (low M_w) BPA-PC as measured via the KBr pellet procedure for solid samples. Notice the absence of phenolic –OH stretches (3600 – 3250 cm^{-1}) and presence of C=O stretches (1782 – 1772 cm^{-1}).

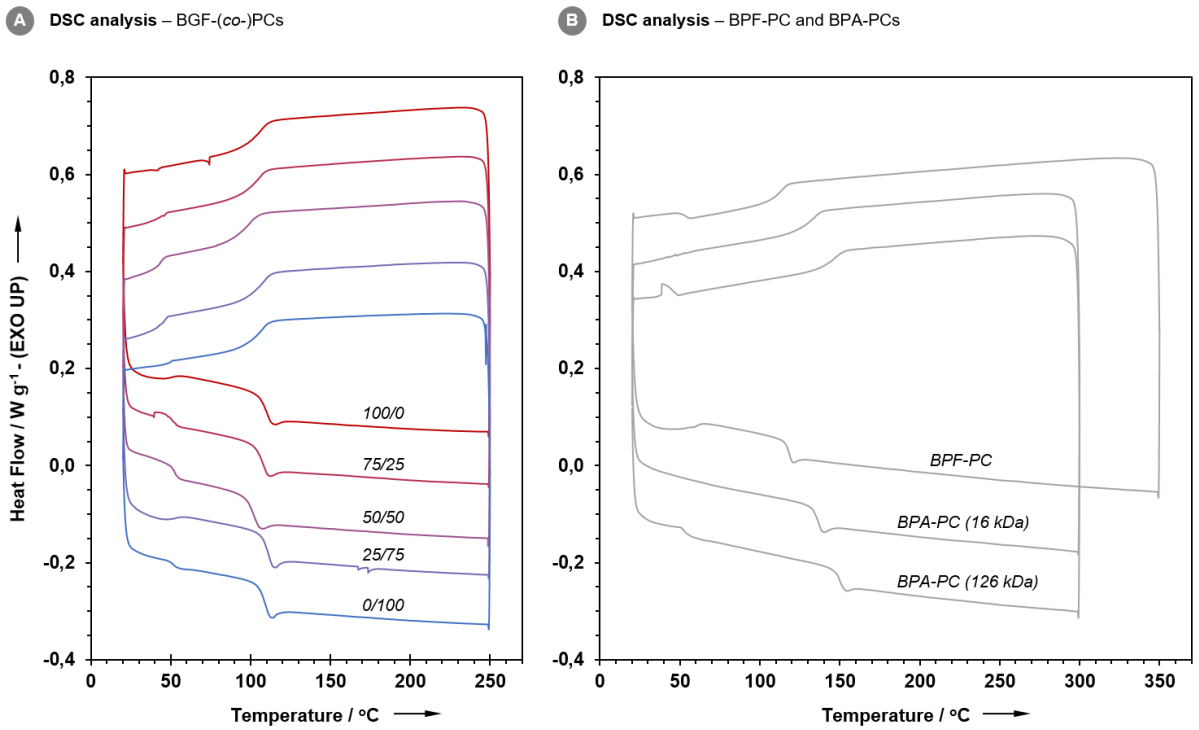

Fig. S14 | DSC traces of (**A**) BGF-(*co*-)PC, and (**B**) BPF-PC and BPA-PCs from 2nd heating/cooling cycle at 10 °C·min^{-1} under N_2. Note that the heat flow values are offset with a multiple of +0.1 W·g^{-1} relative to '0/100' and 'BPA-PC (126 kDa)'. The latter reference itself is offset with +0.1 W·g^{-1} as well.

III. Tables

Table S1. Additional experimental details of the *in vitro* oestrogenic transactivation assay

Compound	Range tested [M][a]		Cytotoxicity
	min.	*max.*	[M][b]
17β-E2	$4.57 \cdot 10^{-13}$	$1.00 \cdot 10^{-9}$	–
p,p'-BPA	$1.00 \cdot 10^{-10}$	$1.00 \cdot 10^{-3}$	$1.00 \cdot 10^{-3}$
p,p'-BPF	$1.00 \cdot 10^{-11}$	$1.00 \cdot 10^{-3}$	$1.00 \cdot 10^{-3}$
p,p'-BGF[c]	$1.00 \cdot 10^{-10}$	$1.00 \cdot 10^{-3}$	$1.00 \cdot 10^{-3}$
m,p'-BGF[c]	$1.00 \cdot 10^{-10}$	$1.00 \cdot 10^{-3}$	$1.00 \cdot 10^{-3}$

[a] Maximum range in preliminary test, range is refined and more narrow in repeat tests. [b] Lowest concentration with cytotoxicity by lactate dehydrogenase (LDH) assay (CytoTox-ONE™ assay) and/or visual microscopy. [c] Top and/or bottom value constrained.

Table S2. Detailed TGA data of BGF-(*co*-)PC benchmarked against BPA-PC, BPF-PC and BGA-PC.[a]

Type of (co)polymer	$T_{d,5\%}$ [°C]	$T_{d,10\%}$ [°C]	$T_{d,50\%}$ [°C]	$T_{d,max}$ [°C]
p,p'-BPA-PC	446	456	496	498
p,p'-BPA-PC[b]	411	431	475	474
p,p'-BPF-PC	402	427	524	447
p,p'-BGF-PC	363	386	422	418
BGF-*co*-PC (25%)[c]	355	384	430	417
BGF-*co*-PC (50%)[c]	336	381	419	417
BGF-*co*-PC (75%)[c]	372	389	421	419
m,p'-BGF-PC	361	385	420	417
p,p'-BGA-PC[d]	n.r.[e]	406	n.r.[e]	436

[a] Calculated by TGA upon heating at 10 °C·min^{-1} under N_2. [b] Reaction stopped after 1h. [c] Percent of *m,p'*-BGF. [d] Literature values.[7] [e] n.r.: not reported.

References

1. H. Witters, A. Freyberger, K. Smits, C. Vangenechten, W. Lofink, M. Weimer, S. Bremer, P. H. J. Ahr and P. Berckmans, *Reproductive Toxicol.*, 2010, **30**, 60-72.
2. P. Balaguer, F. François, F. Comunale, H. Fenet, A.-M. Boussioux, M. Pons, J.-C. Nicolas and C. Casellas, *Sci. Total Environ.*, 1999, **233**, 47-56.
3. P. Berckmans, H. Leppens, C. Vangenechten and H. Witters, *Toxicol. In Vitro*, 2007, **21**, 1262-1267.
4. S.-F. Koelewijn, S. Van den Bosch, T. Renders, W. Schutyser, B. Lagrain, M. Smet, J. Thomas, W. Dehaen, P. Van Puyvelde, H. Witters and B. F. Sels, *Green Chem.*, 2017, **19**, 2561-2570.
5. D. R. Dimmel, D. Shepard and T. A. Brown, *J. Wood Chem. Technol.*, 1981, **1**, 123-146.
6. E. D. Hernandez, A. W. Bassett, J. M. Sadler, J. J. La Scala and J. F. Stanzione III, *ACS Sustain. Chem. Eng.*, 2016, **4**, 4328-4339.
7. G. Chandra, E. J. Nesakumar, V. R. G. Bhotla, S. G. Shetty, J. Mahood, R. R. Gallucci, J. H. Kamps and M. S. Kumar*, US Pat,* 9120893B1, 2015.